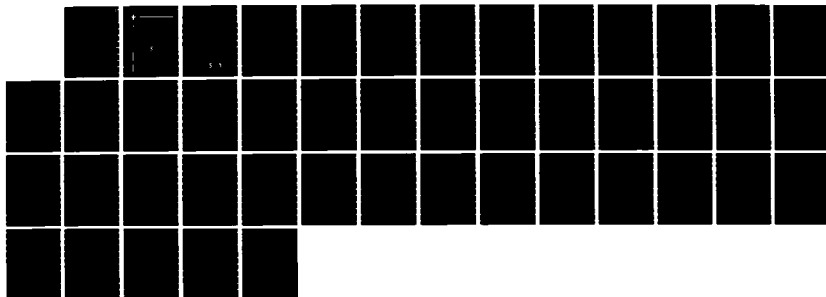AD-A169 117   A FINITE ELEMENT METHOD FOR LOCALIZED FAILURE ANALYSIS   1/1
               (U) BROWN UNIV PROVIDENCE RI DIV OF ENGINEERING
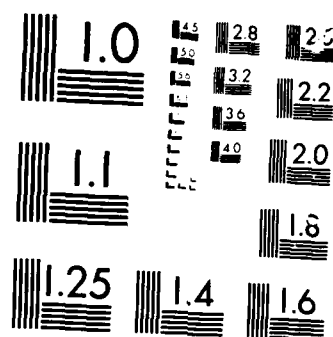   M ORTIZ ET AL. 15 APR 86 N00014-85-K-0720

UNCLASSIFIED   F/G 12/1   NL

Brown University

DIVISION OF ENGINEERING

PROVIDENCE, R.I. 02912

A FINITE ELEMENT METHOD
FOR LOCALIZED FAILURE ANALYSIS

by

Michael Ortiz, Yves Leroy and Alan Needleman
Division of Engineering
Brown University
Providence, RI 02912 USA

DTIC
S ELECTE
JUN 2 3 1986
D

86   5   27   102

$, \quad \nearrow \; 2$

A FINITE ELEMENT METHOD
FOR LOCALIZED FAILURE ANALYSIS

by

Michael Ortiz, Yves Leroy and Alan Needleman
Division of Engineering
Brown University
Providence, RI 02912 USA

April 1986

DTIC
SELECTED
JUN 2 3 1986
D
D

A FINITE ELEMENT METHOD FOR LOCALIZED FAILURE ANALYSIS

Michael ORTIZ, Yves LEROY and Alan NEEDLEMAN

Division of Engineering, Brown University

Providence, Rhode Island 02912, USA

A method is proposed which aims at enhancing the performance of general classes of elements in problems involving strain localization. The method exploits information concerning the process of localization which is readily available at the element level. A bifurcation analysis is used to determine the geometry of the localized deformation modes. When the onset of localization is detected, suitably defined shape functions are added to the element interpolation which closely reproduce the localized modes. The extra degrees of freedom representing the amplitudes of these modes are eliminated by static condensation. The proposed methodology can be applied to 2D and 3D problems involving arbitrary rate-independent material behavior. Numerical examples demonstrate the ability of the method to resolve the geometry of localized failure modes to the highest resolution allowed by the mesh.

April 15, 1986

A FINITE ELEMENT METHOD FOR LOCALIZED FAILURE ANALYSIS

1. Introduction

A phenomenon that frequently accompanies inelastic deformation is the formation of localized bands of intense straining. This phenomenon of localization occurs in a wide variety of solids; in ductile single crystals, Chang and Asaro [1], in structural metals, Costin et al. [2], Cox and Low [3], in saturated clays, Vardoulakis [4,5], in rocks, Waversik and Brace [6] and in concrete, van Mier [7]. The physical mechanisms responsible for triggering localization vary widely. For example, at high rates of loading in structural metals, thermal softening plays a key role in initiating localization [2]. Localization also occurs in metals at low rates of loading. where thermal effects are negligible. [1,3]. Once localization takes place. large strains can accumulate inside the band and lead to fracture.

It is important to note that a concentration of deformation into a more or less well defined band does not necessarily constitute localization in the sense used here. We use the term localization to refer to situations in which the concentration of deformation into a band emerges as an outcome of the constitutive behavior of the material. Accordingly, the orientation of the band is characteristic of the material, rather than a consequece of boundary conditions. We will refer to such a band of localized deformation as a shear band, although in general dilatation as well as shear takes place within the band.

Since large strains accumulate inside a shear band without substantially affecting the strains in the surrounding material. e. g. Hutchinson and Tvergaard [8] and Saje et al. [9], shear bands can only be accurately described by a conventional displacement finite element method if the band interfaces follow element boundaries. Furthermore, the mesh sets the minimum band thickness at one element width. Thus. in order to accurately resolve a narrow shear band, small elements are required. with element boundaries that follow band directions. Finite element analyses of shear bands based on fine meshes of quadrilateral elements built up from four constant strain triangles have given sharply localized deformation modes, see e. g. Tvergaard et al. [10], Tvergaard [11] and the review of Needleman and Tvergaard [12]. A material instability analysis. Hadamard [13], Hill [14], Mandel [15], Thomas [16], Rice [17], is used to orient the quadrilaterals. Localization is found in numerical calculations even when the mesh

2

in not optimally designed, as discussed in [10], but with a certain delay and with some mesh induced shear band broadening.

In a two dimensional rectangular mesh, quadrilaterals built up of four crossed triangles can resolve narrow bands of deformation in four directions; parallel with the sides of the quadrilateral and with the element diagonals. By way of contrast, isoparametric quadrilaterals can only resolve such narrow bands parallel with the element sides. Finite element analyses of oblique localized deformation bands using isoparametric quadrilateral elements, e. g. Prevost and Hughes [18], Prevost [19], Willam et al. [20], do exhibit the tendency for shear bands to form when appropriate critical conditions are reached but have not exhibited the sharp localization obtained using crossed triangles.

However, the crossed triangle finite element formulation is specifically geared to two dimensional problems and it does require careful mesh design to account for likely directions of localization. In this paper a method is proposed which aims at enhancing the performance of isoparametric elements in problems involving strain localization. The formulation here is restricted to small displacement gradient theory and to rate independent constitutive relations. The method uses a material instability bifurcation analysis [13-17], carried out at the element level, to determine the geometry of the ensuing localized deformation modes. When the onset of localization is detected, the element interpolation is extended by adding to it suitably defined shape functions that reproduce the localized deformation modes. These additional shape functions render the element incompatible, but we show that the element satisfies the patch test, Irons [21], Taylor et al. [22]. The extra degrees of freedom representing the amplitudes of the localized modes are eliminated by static condensation. It should be emphasized that all these operations can be implemented at the element level. The proposed methodology can be applied to two and three dimensional problems and does not require a mesh design to take explicit account of likely directions of localization. Pietruszcak and Mroz [23] previously incorporated a shear band mode of deformation into a finite element formulation. However, in their approach, the localized shear band is specified by the consitutive relation as the sole mode of inelastic deformation and the element strain rates are directly given in terms of conventional shape functions.

3

Numerical results are presented in Section 4 for localization in both nearly incompressible solids and in compressible solids. Even in the absence of shear bands, isoparametric elements are of limited value for nealy incompressible solids, such as the classical plastic solid. Mesh locking occurs as a result of the near incompressibilit y in the fully plastic range, Nagtegaal et al. [24]. This difficulty can be overcome through the use of a method to handle internal constrains; for example, here we use a $\bar{\mathbf{B}}$ technique, Hughes [25]. It bears emphasis, however, that to resolve localized deformation patterns in a nearly incompressible solid it is necessary, but not sufficient, to prevent mesh locking. Our numerical results show that the enhanced element introduced here does resolve localization more sharply than the underlying $\bar{\mathbf{B}}$-isoparametric element. Also, for compressible solids, where mesh locking due to incompressibilit y is not an issue. numerical results are presented that illustrate the improved performance of the enhanced element.

2. Localization of as a Bifurcation Phenomenon

In this section we review some aspects of the general theory of localization of inelastic deformations. Some of the basic principles underlying the theory follow from Hadamard's studies of elastic stability [13], extended to the inelastic context by Thomas [16], Hill [14], Mandel [15] and Rice [17]. Here, for simplicity attention is confined to infinitesimal deformations and thermally decoupled, rate-independent material behavior.

Consider a homogeneous, homogeneously deformed solid subjected to quasi-static incre-ments of deformation $\dot{\epsilon}$. We wish to determine if a *bifurcation* can occur in such a manner that subsequent deformations become discontinuous across a plane of orientation $\mathbf{n}$. Let $\mathbf{u}$ be the displacement field in the solid. Whereas $\mathbf{u}$ itself remains continuous after the onset of local-ization, the displacement gradients $\nabla \mathbf{u}$ will exhibit a jump across the plane of discontinuity, i. e.,

$$[\![u_{i,j}]\!] \equiv u_{i,j}^{+} - u_{i,j}^{-} \neq 0 \tag{1}$$

where the superindex '+' refers to the plus side of the plane of discontinuity and '−' to the minus side. Maxwell's compatibilit y conditions necessitate that the jump (1) be of the form

$$[\![u_{i,j}]\!] = g_i n_j \tag{2}$$

4

for some vector g. Let us further define **m** to be the unit vector along g, i. e.,

$$m_i \equiv g_i/g, \qquad g \equiv |\mathbf{g}| \qquad (3)$$

The pair of unit vectors **m** and **n** entirely define the nature of the discontinuity. The corresponding strain jump is given by

$$[\![\epsilon_{ij}]\!] = (g_i n_j + g_j n_i)/2 \qquad (4)$$

Often, two parallel planes of discontinuity pair up to form a band of instensely deformed material. Two limiting cases are noteworthy:

(a) **m** *orthogonal to* **n**. The material in the band deforms in simple shear, i. e, a *shear band* develops.

(b) **m** *parallel to* **n**. The band undergoes extension normal to the planes of discontinuity. In certain circumstances this can be interpreted as a *splitting* failure mode.

Shear bands are characteristic of materials exhibiting isochoric plasticity. On the other hand, splitting failure modes can be thought of as idealizations of the separation processes which occur during progressive brittle failure. In between these two extremes lies a continuous spectrum of mixed failure modes for which **m** and **n** are neither orthogonal nor parallel. Plastic-fracturing materials such as concrete, rocks and ceramics are capable of failing in mixed modes, with the angle between **m** and **n** lying anywhere from $0°$ to $90°$ [17,26,27].

We next investigate under what conditions localized failure modes are possible. To this end, let us assume that the solid is at the onset of localization. At this point, the stresses $\boldsymbol{\sigma}$ and strains $\boldsymbol{\epsilon}$ are continuous throughout the body. However, the stress and strain rates $\dot{\boldsymbol{\sigma}}$ and $\dot{\boldsymbol{\epsilon}}$ will exhibit discontinuities across a plane whose orientation is to be determined. Assuming rate-independent material behavior the incremental stress-strain relations take the form

$$\dot{\sigma}_{ij} = D_{ijkl}\dot{\epsilon}_{kl} \qquad (5)$$

where **D** is the tangent stiffness tensor for the material. Rate independence implies that **D** is homogeneous of degree zero in $\dot{\epsilon}$. We restrict attention to cases where **D** is piecewise independent

5

of $\dot{\epsilon}$. For example, in classical plasticity **D** has two branches, one corresponding to plastic loading, the other to elastic unloading.

For elastic-plastic solids, the localization bifurcation analysis is carried out using the same branch of the moduli **D** across the incipient planes of discontinuity, which corresponds to investigating bifurcation for a *linear comparison solid*, Hill [33], Raniecki and Bruhns [34]. Hence, taking jumps in (5) leads to

$$[\![\dot{\sigma}_{ij}]\!] = D_{ijkl}[\![\dot{\epsilon}_{kl}]\!] \tag{6}$$

Equilibrium across the discontinuity planes requires that the tractions **t** be continuous, i. e.,

$$[\![\dot{t}_j]\!] = [\![n_i \dot{\sigma}_{ij}]\!] = n_i [\![\dot{\sigma}_{ij}]\!] = 0 \tag{7}$$

Combining (6) and (7). it follows that

$$n_i D_{ijkl}[\![\dot{\epsilon}_{kl}]\!] = 0 \tag{8}$$

Finally, using the kinematic relation (4) and the definition (3) we obtain

$$A_{jk}(\mathbf{n})m_k = (n_i D_{ijkl} n_l)m_k = 0 \tag{9}$$

This condition has to be satisfied by **m** and **n** for the localized mode to be possible. The onset of localization occurs at the first point in the deformation history for which a nontrivial solution of (9) exists. For localization to occur along the direction **n**, the localization matrix **A(n)** has to have at least one zero eigenvalue. This in turn necessitates

$$f(\mathbf{n}) \equiv det(\mathbf{A}(\mathbf{n})) = 0 \tag{10}$$

If a unit vector **n** satisfying (10) can be found. the corresponding vector **m** which completes the definition of the localized mode follows from (9).

A numerical procedure for computing **m** and **n** from the above equations is given in Appendix I. In two dimensions, the localization angles can be computed directly as the roots of a cubic polynomial, while in three dimensions the localization directions are computed iteratively.

An example of application of the solution procedure to complex three-dimensional constitutive equations is found in [27].

3. An Assumed Strain Finite Element Method for Localized Failure Analysis

It has been long recognized [10], that isoparametric elements face inherent limitations in the presence of localized deformations. The essence of the problem can be illustrated by means of Fig. 1, which shows a shear band traversing a regular mesh at 45°. The elements on the boundary of the shear band should exhibit a strain discontinuity. However, such a deformation pattern is not well represented within the isoparametric interpolation. On the contrary, the element tries to conform to the deformation field by averaging the deformation on both sides of the discontinuity. As a result, the true discontinuous behavior may be smeared out over several elements or in some cases precluded altogether.

A numerical procedure which circumvents these difficulties is proposed next. For simplicity, attention is confined to infinitesimal deformations. The method can be described as follows:

(i) For every element in the mesh a localization analysis of the type described in Section 2 is carried out at the reduced quadrature points, where the stresses and other state variables are computed most accurately [35]. For instance, in 4-node and 9-node isoparametric elements localization is investigated at the centroid and the 2×2 Gauss points, respectively. This analysis is repeated at every step of the solution process until the onset of localization is detected at one or more reduced quadrature points.

(ii) From this point on, suitable deformation modes which exactly reproduce the discontinous deformation patterns are added to the element or elements where localization is detected. The extra degrees of freedom are eliminated at the element level by means of static condensation.

This approach takes advantage of the fact that considerable information concerning the localization process can be readily obtained at the element level. The method aims at utilizing this information to enhance the performance of the element in the presence of localized failure.

3.1 Localized deformation modes

We envision a generic element in which the displacement field is interpolated as

7

$$u_i(\mathbf{x}) = \sum_{a=1}^{N} u_{ia} N_a(\mathbf{x}) \tag{11}$$

where u_{ia} are the nodal displacements, $N_a(\mathbf{x})$ are the interpolation functions and the sum extends to all N nodes in the element. A typical example is given by the serendipity family of 4 to 9 node isoparametric elements. Let us further denote by $\{\xi_{ir}, r = 1, \ldots, NQ\}$ the coordinates of the reduced quadrature points. Here the subindex r ranges over all NQ reduced quadrature points in the element.

Based on the state variables computed at the points ξ_r a localization analysis of the type described in Section 2 can be carried throughout the solution process. Let us assume that in the generic element under consideration and at some stage of the solution several bifurcations have been detected resulting in NL localized modes. The geometry of these deformation modes is fully determined by pairs of unit vectors $\{(m_{ia}, n_{ia}), \alpha = 1, \ldots, NL\}$ representing the displacement direction and the normal to the surface of discontinuity, respectively. Furthermore, let ξ_a denote the reduced quadrature point at which the αth localized mode has been detected.

Localized deformation modes exhibit a strain discontinuity along the surface of normal n_a, passing through ξ_a. In order to accommodate these deformation modes, we extend the element interpolation by means of suitably defined shape functions which closely reproduce the localized deformation patterns. To this end, for each localized mode we define the functions

$$M_{ia}^+(\mathbf{x}) = \begin{cases} m_{ia} [\mathbf{n}_a \cdot (\mathbf{x} - \xi_a)], & \text{if } \mathbf{n}_a \cdot (\mathbf{x} - \xi_a) \geq 0; \\ 0, & \text{otherwise.} \end{cases} \tag{12}$$

and

$$M_{ia}^-(\mathbf{x}) = \begin{cases} -m_{ia} [\mathbf{n}_a \cdot (\mathbf{x} - \xi_a)], & \text{if } \mathbf{n}_a \cdot (\mathbf{x} - \xi_a) \leq 0; \\ 0, & \text{otherwise.} \end{cases} \tag{13}$$

where no sum is implied on the index α. These functions exhibit a jump across the surface of discontinuity

$$[\![(M_{ia}^+)_{,j}]\!] = [\![(M_{ia}^-)_{,j}]\!] = m_{ia} \, n_{ja} \tag{14}$$

Consequently, any convex combination

8

$$M_{i\alpha}(\mathbf{x}) = (1 - \lambda_\alpha)M_{i\alpha}^-(\mathbf{x}) + \lambda_\alpha M_{i\alpha}^+(\mathbf{x}) \tag{15}$$

of $M_{i\alpha}^+$ and $M_{i\alpha}^-$ exhibits the same jump (14). Thus, (15) defines a one-parameter family of possible shape functions for the localized modes. Adding these shape functions to the element interpolation, the local displacement field becomes

$$u_i(\mathbf{x}) = \sum_{a=1}^{N} u_{ia} N_a(\mathbf{x}) + \sum_{\alpha=1}^{NL} \gamma_\alpha M_{i\alpha}(\mathbf{x}) \tag{16}$$

where $\{\gamma_\alpha, \ \alpha = 1, \ldots, NL\}$ are the amplitudes of the localized modes. It should be noted that shape functions (15) are *incompatible*, i. e., in general do not satisfy the C^0 continuity requirement across the element boundary and the element becomes *nonconforming*.

The element strain field is computed from (16) to be

$$\epsilon_{ij}(\mathbf{x}) = \left(u_{i,j}(\mathbf{x}) + u_{j,i}(\mathbf{x})\right)/2 = \sum_{a=1}^{N} \left(u_{ia} N_{a,j}(\mathbf{x}) + u_{ja} N_{a,i}(\mathbf{x})\right) + \sum_{\alpha=1}^{NL} \gamma_\alpha \left((M_{i\alpha})_{,j}(\mathbf{x}) + (M_{j\alpha})_{,i}(\mathbf{x})\right) \tag{17}$$

For subsequent derivations it proves convenient to recast this expression in matrix form. Let $\mathbf{u}_1$ denote the nodal displacement array and $\mathbf{u}_2$ the collection of amplitudes γ_α of the additional incompatible modes. Then (17) can be expressed in the more compact form

$$\boldsymbol{\epsilon}(\mathbf{x}) = \mathbf{B}_1 \mathbf{u}_1 + \mathbf{B}_2 \mathbf{u}_2 \tag{18}$$

It follows from (12) and (15) that the compatibility matrix $\mathbf{B}_2$ takes the form

$$(\mathbf{B}_2)_{ij\alpha} = \begin{cases} \lambda_\alpha (m_{i\alpha} n_{j\alpha} + m_{j\alpha} n_{i\alpha})/2, & \text{if } \mathbf{n}_i \cdot (\mathbf{x} - \boldsymbol{\xi}_i) > 0; \\ -(1 - \lambda_\alpha)(m_{i\alpha} n_{j\alpha} + m_{j\alpha} n_{i\alpha})/2, & \text{if } \mathbf{n}_i \cdot (\mathbf{x} - \boldsymbol{\xi}_i) < 0. \end{cases} \tag{19}$$

so that the element strain field exhibits a jump

$$[\![\epsilon_{ij}(\mathbf{x})]\!] = \gamma_\alpha (m_{i\alpha} n_{j\alpha} + m_{j\alpha} n_{i\alpha})/2 \tag{20}$$

across the αth surface of discontinuity. Thus, the parameters γ_α represent the magnitude of the strain discontinuity associated with the αth localized mode.

It is implied in (18) that in the absence of localized modes the element strain field takes the form $\boldsymbol{\epsilon}(\mathbf{x}) = \mathbf{B}_1(\mathbf{x})\mathbf{u}_1$, where $\mathbf{B}_1$ results from applying the strain-displacement relations to the conforming interpolation (11). It was noted in [24] that in applications involving isochoric perfect plasticity this formulation results in an overly stiff response due to the poor handling by the element of the near-incompressibily which accompanies extensive plastic flow. A number of techniques have been proposed to alleviate the locking phenomena associated with internal constraints such as incompressibility. In this work we adopt Hughes' $\bar{\mathbf{B}}$-method [25] which for the 4-node quadrilateral consists of replacing the compatibility matrix $\mathbf{B}_1$ by a modified $\bar{\mathbf{B}}_1$ of the form

$$\bar{\mathbf{B}}_1(\mathbf{x}) \equiv \mathbf{B}_1^{dev}(\mathbf{x}) + \epsilon \mathbf{B}_1^{vol}(\mathbf{x}) + (1 - \epsilon)\mathbf{B}_1^{vol}(\mathbf{x}_c) \tag{21}$$

Here, $\mathbf{B}_1^{dev}$ and $\mathbf{B}_1^{vol}$ are defined so as to give the deviatoric and volumetric parts of the strain tensor when multiplied by $\mathbf{u}_1$, $\mathbf{x}_c$ is the centroid of the element and ϵ is a small stabilization parameter which is included to suppress spurious pressure modes [28]. For the 9-node element, $\mathbf{B}_1^{vol}$ is computed at the reduced quadrature points and extrapolated to the rest of the element by means of suitable shape functions. Hughes' $\bar{\mathbf{B}}$-method is closely related to selective reduced integration techniques and to mixed methods, see e. g. the review of Hughes et al. [29].

Substituting $\mathbf{B}_1$ in (18) by the modified compatibility matrix $\bar{\mathbf{B}}_1$ the element strain field finally takes the form

$$\boldsymbol{\epsilon}(\mathbf{x}) = \bar{\mathbf{B}}_1\mathbf{u}_1 + \mathbf{B}_2\mathbf{u}_2 \tag{22}$$

Let us define the stiffness submatrices

$$\mathbf{K}_{11} = \int_{\Omega^e} \bar{\mathbf{B}}_1^T \mathbf{D}\bar{\mathbf{B}}_1 \, dV$$

$$\mathbf{K}_{12} = \mathbf{K}_{21}^T = \int_{\Omega^e} \bar{\mathbf{B}}_1^T \mathbf{D}\mathbf{B}_2 \, dV \tag{23}$$

$$\mathbf{K}_{22} = \int_{\Omega^e} \mathbf{B}_2^T \mathbf{D}\mathbf{B}_2 \, dV$$

where Ω^e signifies the domain of the element and $\mathbf{D}$ are the tangent stiffness tensor of the material. Since the localized modes represent internal degrees of freedom of the element, the corresponding amplitudes $\mathbf{u}_2$ can be eliminated by static condensation [30] to obtain

10

$$\dot{\mathbf{u}}_2 = - \mathbf{K}_{21} \mathbf{K}_{22}^{-1} \dot{\mathbf{u}}_1 \tag{24}$$

and the effective element stiffness becomes

$$\mathbf{K} = \mathbf{K}_{11} - \mathbf{K}_{12} \mathbf{K}_{22}^{-1} \mathbf{K}_{21} \tag{25}$$

It should be emphasized that all the matrix operations indicated in (25) can be carried out at the element level.

As can be seen from (25), in the present method the stiffness matrix $\mathbf{K}_{11}$ of the underlying conforming element is modified by means of a term which represents the net effect of the added localized modes. In Section 4 it is shown by way of numerical examples that the enhanced element is more conducive to localization and provides sharper results than those obtained from the $\bar{\mathbf{B}}$-method alone.

3.2 Patch test

In Section 3.1 it was noted that the introduction of localized deformation modes renders the element nonconforming. To insure that the convergence properties of the underlying conforming element are not altered, the incompatible modes have to be defined in such a way that the patch test is satisfied. This test determines whether or not the element consistently reproduces states of constant strain. If so, convergence takes place within each element, e. g. Strang and Fix [28].

The definition of shape functions (15) contains a set of free, as yet undetermined parameters λ_a . Next, it is shown that the value of these parameters can be uniquely determined from the requirement that the element satisfy the patch test. Taylor et al. [22] derived a necessary condition for the patch test to be passed by a nonconforming element. With the present notation such condition reads

$$\int_{\Omega^e} \mathbf{B}_2 \, dV = \mathbf{0} \tag{26}$$

In view of (19), (26) necessitates

$$[-(1 - \lambda_a) A_a^{c-} + \lambda_a A_a^{c+}](m_{ia} n_{ja} + m_{ja} n_{ia})/2 = 0 \tag{27}$$

11

where A_{a}^{r+} and A_{a}^{r-} are the areas of the element subdomains lying on the plus and the minus sides of the αth surface of discontinuity, respectively. Condition (27) is satisfied by setting

$$-(1 - \lambda_a)A_a^{r-} + \lambda_a A_a^{r+} = 0 \qquad (28)$$

which yields

$$\lambda_a = \frac{A_a^{r-}}{A^r} \qquad (29)$$

where $A^r = A_a^{r+} + A_a^{r-}$ is the total area of the element. In practice, satisfactory results are obtained by computing the areas A_a^{r+} and A_a^{r-} by numerical integration.

3.3 Formulation as an assumed strain method

A broad class of finite element schemes commonly referred to as $\bar{B}$-methods consist of postulating a relation $\epsilon = \bar{B}u$ for some suitably defined operator $\bar{B}$ and a tangent stiffness matrix of the form

$$\mathbf{K} = \int_{\Omega^e} \bar{\mathbf{B}}^T \mathbf{D} \bar{\mathbf{B}} dV \qquad (30)$$

This class of methods originated with the pioneering paper of Hughes [25] and have been particularly successful in overcoming mesh locking difficulties associated with internal constraints. The formulation proposed here can be rephrased as a $\bar{B}$-method by noting that (25) can be alternatively expressed as

$$\mathbf{K} = \int_{\Omega^e} (\bar{\mathbf{B}}_1 - \mathbf{K}_{12} \mathbf{K}_{22}^{-1} \mathbf{B}_2)^T \mathbf{D} (\bar{\mathbf{B}}_1 - \mathbf{K}_{12} \mathbf{K}_{22}^{-1} \mathbf{B}_2) dV \qquad (31)$$

Comparison of (30) and (31) warrants the identification

$$\bar{\mathbf{B}} \equiv \bar{\mathbf{B}}_1 - \mathbf{K}_{12} \mathbf{K}_{22}^{-1} \mathbf{B}_2 \qquad (32)$$

Thus, the proposed formulation can be regarded as a $\bar{B}$-method in which the the compatibility operator is postulated to take the form (32).

The expression (31) for the effective stiffness matrix can be directly obtained from the Hellinger-Reissner variational principle. This principle characterizes the equilibrium and compatibility equations as the Euler equations of the potential

12

$$L(\dot{\mathbf{u}}, \dot{\boldsymbol{\epsilon}}) = \int_{\Omega} \left[\frac{1}{2} D_{ijkl} \dot{\epsilon}_{ij} (\dot{u}_{i,j} + \dot{u}_{j,i}) - \frac{1}{2} D_{ijkl} \dot{\epsilon}_{ij} \dot{\epsilon}_{kl} - \dot{f}_i \dot{u}_i \right] dV - \int_{\partial\Omega_{\tau}} \dot{t}_i \dot{u}_i \, dS \qquad (33)$$

where Ω is the domain occupied by the body, $\partial\Omega_{\tau}$ is the traction boundary and $\mathbf{f}$ and $\mathbf{t}$ denote the body forces and applied tractions, respectively. Guided by the results obtained from the static condensation procedure we postulate the following two-field interpolation for displacements and strains

$$u_i(\mathbf{x}) = \sum_{a=1}^{N} u_{ia} N_a(\mathbf{x})$$
$$\dot{\boldsymbol{\epsilon}}(\mathbf{x}) = \bar{\mathbf{B}} \dot{\mathbf{u}}_1 = (\bar{\mathbf{B}}_1 - \mathbf{K}_{12} \mathbf{K}_{22}^{-1} \mathbf{B}_2) \dot{\mathbf{u}}_1 \qquad (34)$$

where, as before, $\mathbf{u}_1$ denotes the collection of nodal displacements u_{ia} and N_a are the conformal shape functions. Substituting the interpolated fields (34) into the Hellinger-Reissner potential the discretized Euler equations are found to be

$$\sum_e \left[\int_{\Omega^e} \mathbf{B}_1^T \mathbf{D} \bar{\mathbf{B}} dV \right] \dot{\mathbf{u}}_1 = \sum_e \dot{\mathbf{f}}_1$$
$$\left[\int_{\Omega^e} \bar{\mathbf{B}}^T \mathbf{D} (\mathbf{B}_1 - \bar{\mathbf{B}}) dV \right] \dot{\mathbf{u}}_1 = \mathbf{0} \qquad (35)$$

where the element forces are given by

$$(\dot{\mathbf{f}}_1)_{ia} = \int_{\Omega^e} \dot{f}_i N_a \, dV + \int_{\partial\Omega_{\tau}^e} \dot{t}_i N_a \, dS \qquad (36)$$

It is interesting to note that only the conformal shape functions are involved in the computation of the element forces. It follows from (35a) that the element stiffness matrix takes the form

$$\mathbf{K} = \int_{\Omega^e} \mathbf{B}_1^T \mathbf{D} \bar{\mathbf{B}} dV \qquad (37)$$

On the other hand, satisfaction of eq. (35b) for arbitrary incremental displacements necessitates

$$\int_{\Omega^e} \bar{\mathbf{B}}^T \mathbf{D} (\mathbf{B}_1 - \bar{\mathbf{B}}) dV = \mathbf{0} \qquad (38)$$

If this condition is identically satisfied the stiffness matrix (37) can be alternatively expressed in $\bar{\mathbf{B}}$-form

13

$$\mathbf{K} = \int_{\Omega^e} \bar{\mathbf{B}}^T \mathbf{D} \bar{\mathbf{B}} dV \tag{39}$$

A simple computation reveals that for the present choice of $\bar{\mathbf{B}}$-matrix (35b) condition (38) is indeed identically satisfied. Hence the method can be directly derived from the Hellinger-Reissner variational principle. The conditions under which a $\bar{\mathbf{B}}$-method is variationally consistent were first elucidated in [31] where orthogonality conditions (38) were derived within the more general context of the Hu-Washizu principle.

Satisfaction of orthogonality conditions (38) not only places the method on a solid variational foundation but also has a consequence of some practical importance. Eq. (35a) indicates that the internal forces evolve at a rate

$$\dot{\mathbf{f}}_1^{nt} = \sum_r \left[\int_{\Omega^r} \mathbf{B}_1^T \mathbf{D} \bar{\mathbf{B}} dV \right] \dot{\mathbf{u}}_1 \tag{40}$$

Integrating in time we obtain the expression

$$\mathbf{f}_1^{nt} = \sum_r \int_{\Omega^r} \mathbf{B}_1^T \boldsymbol{\sigma} dV \tag{41}$$

Thus, the internal forces can be computed by using the conformal compatibility matrix $\mathbf{B}_1$ regardless of whether localized deformation modes have been added to the interpolation. On one hand, this has the effect of eliminating the overhead involved in computing the enhanced $\bar{\mathbf{B}}$-matrix during the computation of the internal forces. Secondly, eq. (41) guarantees that as long as the stress history is continuous in time the internal forces will also be a continuous function of time. In particular, no sudden jumps will be experienced by the internal forces on adding a localized mode to the interpolation.

4. Numerical Examples

Considerable insight into the performance of the method can be obtained by examining the behavior of a single element. A first simple example of this nature is shown in Fig. 2. The problem concerns one element in which three nodes are constrained in both directions while displacements are prescribed on the fourth node which result in nonuniform shear across the element. The computed force-displacement diagrams corresponding to an isoparametric element, Hughes' $\bar{\mathbf{B}}$-method and the present approach are shown in Fig. 2. It is seen that the

14

isoparametric element exhibits considerable residual stiffness once the element is fully plastified. By contrast, both the $\bar{\mathbf{B}}$ method and the enhanced element predict limit loads of similar values. Once these limit loads are attained no residual stiffness is observed and a failure mechanism is formed. However, the nature of the failure mechanisms predicted by both methods is significantly different. Fig. 4 shows the computed strain histories at all quadrature points. It is seen that those obtained from the $\bar{\mathbf{B}}$-method show essentially proportional growth and no tendency towards localization. By contrast, in the enhanced element a bifurcation is detected as the centroid plastifies which results in the localized mode shown in Fig. 3. From this point on, the strain within the lower half of the element remains constant and all subsequent deformations are localized to the upper half. Thus, whereas adequate handling of incompressibility suffices to capture limit loads accurately it appears that to obtain sharp predictions of localized failure further structure has to be added to the element.

A second example is concerned with shear band formation in a perfectly plastic von Mises solid with a periodic array of inhomogeneities, Fig. 5. The body is subjected to an overall uniform shear deformation. The inhomogeneities are modelled by one element voids which act as nucleation sites from where shear bands emanate. The material parameters used in the analysis are $E = 2 \times 10^5$, $\nu = 0.3$ and $\sigma_y = 200$, where E, ν and σ_y are the Young's modulus, Poisson's ratio and yield stress, respectively. Fig. 6 shows the deformed mesh corresponding to a prescribed overall shear deformation $\bar{\gamma} = 1.6 \times 10^{-3}$. A shear band spanning the inhomogeneities is clearly apparent. The bifurcated elements and localization directions are shown in Fig. 7. It is seen that localization is confined to a diagonal band two elements wide. Fig. 8 shows the distribution of equivalent plastic strain across the center of the shear band computed from the $\bar{\mathbf{B}}$-method and the enhanced element at two stages of the solution process. Again it is seen that the enhanced element results in a sharper shear band with higher amounts of plastic deformation concentrated over a narrower region than the $\bar{\mathbf{B}}$-method.

Our next example concerns a plane strain rigid punch problem and aims at assessing the performance of the method in the presence of curved shear bands. Fig. 9 shows the geometry of the problem and the final deformed mesh for a prescribed displacement $\bar{u} = 0.4$. A perfectly plastic, von Mises model was assumed with material constants $E = 30000$, $\nu = 0.3$ and $\sigma_y = 60$.

15

Fig. 10 shows the contours of maximum shear strains computed from the $\bar{B}$-method and the enhanced element. A well defined shear band is observed in both cases. However, the computed shear strains are seen to be about 50% higher in the case of the enhanced element. Thus, the proposed method is seen to improve the performance of the underlying element regardless of the orientation of the shear band with respect to the mesh.

The examples discussed above show a purely quantitative difference in the response as computed with or without localized modes. Our final example is concerned with a case in which the enhanced element accurately captures a failure mode which the underlying element fails to detect. Here we consider a rectangular plane strain specimen compressed between two rigid platens, Fig. 11. Perfect stick between the specimen and the platens is assumed. The material model used in the calculations is Drucker-Prager's model for soils [32], with a friction angle of 30°, a dilatancy angle of 10° and a cohesion of 5. Perfect plasticity is assumed and the elastic response is taken to be linear and isotropic with $E = 5000$ and $\nu = 0.3$. This constitutive relation falls within the framework analyzed by Rudnicki and Rice [26], and a noteworthy outcome of their instability analysis is that the nonassociated character of the constitutive response has the effect of promoting localization. It should also be emphasized that the material under consideration is plastically dilatant and mesh locking due to near-incompressibility is of no concern. Fig. 12 depicts the load-displacement curve computed from a regular isoparametric element and the same element with localized modes added to the interpolation. As can be seen, both curves are virtually identical during the first stages of loading. However, at some critical deformation the enhanced element exhibits a sudden drop in the load. This corresponds to a bifurcation into the failure mechanism shown in Fig. 13b. By contrast, the isoparametric element appears to preclude the development of a failure mode and the deformation pattern remains essentially unchanged throughout the loading process, Fig. 13a. The distribution of effective plastic strain shown in Fig. 14 further illustrates this discrepancy. Whereas the isoparametric element predicts a smooth distribution of plastic flow over the specimen, Fig. 14b, the enhanced element yields a rather intricate pattern with localized regions of intense straining, Fig. 14a. Since in this example incompressibility is not a issue, it is clear that the inability of the isoparametric element to produce localized failure modes

stems from reasons other than mesh locking. As discussed in Section 3, the smoothness of the isoparametric interpolation and the tendency of the element to smear out strain discontinuities are at the basis of the poor performance.

5. Summary and Conclusions

A method has been presented which aims at enhancing the performance of general classes of elements in problems involving localized failure. The method exploits the fact that considerable information concerning the process of localization can be readily obtained at the element level. A simple analysis suffices to detect the onset of localization in an element and to determine the geometry of the localized deformation modes. This information is utilized to set up additional shape functions which closely reproduce the localized deformation patterns. The additional degrees of freedom are then eliminated at the element level by static condensation. Although the resulting element is nonconforming the patch test is satisfied and the convergence properties of the underlying conforming element are not altered. The method can be formulated as a $\bar{B}$-method or derived directly from the Hellinger-Reissner principle. Numerical examples indicate that whereas limit loads can be accurately computed by means of finite element methods which adequately handle the incompressibility constraint, to obtain sharp predictions of localized failure modes using quadrilateral isoparametric elements further structure has to be added to the interpolation. The present approach provides an efficient means of incorporating this additional structure into general classes of 2D and 3D elements.

Appendix I. Solution of the Localization Condition

In this appendix we discuss a computational procedure for detecting the onset of localization and determining the localization directions m and n. It proves convenient to treat the 2D and 2D cases separately.

Three-dimensional case. If the material response is path-dependent, the integration of the constitutive equations has to be carried out incrementally. If, for instance, the instantaneous initial response of the material is isotropic-elastic, the localization function (10) initially takes the value

$$f(\mathbf{n}) = (\lambda_. + 2\mu_.)\mu_.^2 \tag{A1.1}$$

17

where λ_o and μ_o are the Lamé constants of the virgin material. Note that $f(\mathbf{n}) > 0$ and independent of $\mathbf{n}$. As the process of deformation progresses, f may develop minima which eventually become negative or zero. This in turn signals the onset of localization. To detect precisely when this happens, the minima of the localization function f can be computed at every deformation increment and the localization condition (10) checked at the minima. This leads to considering the constrained minimization problem

$$minimize \quad f(\mathbf{n}) \equiv det\big(n_i\, D_{ijkl}\, n_l\big)$$
$$subject\ to \quad |\,\mathbf{n}\,| = 1 \tag{A1.2}$$

where $\mathbf{D}$ is the current value of the tangent moduli. The minima are characterized by the condition

$$\frac{\partial}{\partial n_i}\big[f(\mathbf{n}) - \lambda\,|\,\mathbf{n}\,|^2\big] = \frac{\partial f(\mathbf{n})}{\partial n_i} - 2\lambda n_i = 0 \tag{A1.3}$$

where λ is a Lagrange multiplier. Differentiating f in (A1.3) one obtains

$$det(\mathbf{A}(\mathbf{n}))D_{ijkl}\,A_{kj}^{-1}(\mathbf{n})n_l - \lambda n_i = 0 \tag{A1.4}$$

Introducing the notation

$$J_{il}(\mathbf{n}) \equiv det(\mathbf{A}(\mathbf{n}))D_{ijkl}\,A_{kj}^{-1}(\mathbf{n}) \tag{A1.5}$$

the minimum condition (A1.4) can be recast as

$$J_{il}(\mathbf{n})n_l - \lambda n_i = 0 \tag{A1.6}$$

The solutions of (A1.6) can be found in two steps:

i) Expressing $\mathbf{n}$ in terms of spherical angles, i. e., setting $\mathbf{n} = (cos\varphi cos\theta,\ cos\varphi sin\theta,\ sin\varphi)$, the range of variation $[0, 2\pi] \times [0, \pi/2]$ of (θ, φ) is swept at 5-degree increments to determine a first approximation $\mathbf{n}^{(0)}$ to the minima.

ii) The locations of the minima are then pinpointed by means of the iterative scheme:

$$J_{il}\big(\mathbf{n}^{(k)}\big)\,n_l^{(k+1)} - \lambda^{(k+1)}\,n_i^{(k+1)} = 0 \tag{A1.7}$$

18

Thus, at every iteration an eigenvalue problem is formulated based on the matrix $\mathbf{J}$ evaluated at the previous iteration $\mathbf{n}^{(k)}$. The minimum eigenvector of (A1.7) is taken as the new iterate $\mathbf{n}^{(k+1)}$.

Once the orientations of the discontinuity planes have been determined, the corresponding m-vectors are computed as the zero-eigenvectors of the localization matrix $\mathbf{A}(\mathbf{n})$.

Two-dimensional case. In the 2D case the localization matrix $\mathbf{A}(\mathbf{n})$ is 2×2 and one readily finds that

$$det\big(\mathbf{A}(\mathbf{n})\big) = a_0\, n_1^4 + a_1\, n_1^3\, n_2 + a_2\, n_1^2\, n_2^2 + a_3\, n_1\, n_2^3 + a_4 \qquad (A1.8)$$

where

$$a_0 = D_{1111} D_{1212} - D_{1112} D_{1211}$$

$$a_1 = D_{1111} D_{1222} + D_{1111} D_{2212} - D_{1112} D_{2211} - D_{1122} D_{1211}$$

$$a_2 = D_{1111} D_{2222} + D_{1112} D_{1222} + D_{1211} D_{2212} - D_{1122} D_{1212} - D_{1122} D_{2211} - D_{1212} D_{2211} \qquad (A1.9)$$

$$a_3 = D_{1112} D_{2222} + D_{1211} D_{2222} - D_{1122} D_{2212} - D_{1222} D_{2211}$$

$$a_4 = D_{1212} D_{2222} - D_{2212} D_{1222}$$

Setting $n_1 = cos\theta$, $n_2 = sin\theta$ in eq. (A1.8) the localization condition becomes

$$f(x) = a_0\, x^4 + a_1\, x^3 + a_2\, x^2 + a_3\, x + a_4 = 0 \qquad (A1.10)$$

where one writes $x = tan\theta$. In general, the polynomial $f(x)$ in (A1.10) is positive everywhere prior to localization. Thus the onset of localization can be determined by simply examining the sign of the minima of $f(x)$. These occur at the roots of the cubic polynomial $f'(x)$ which can be computed in close form by means of Cardan's formulae. As long as the minima of $f(x)$ remain positive localization does not develop. The onset of localization is signaled by one of more minima of $f(x)$ crossing the x-axis.

Acknowledgements

References

1. Chang, Y. W. and Asaro, R. J., "An Experimental Study of Shear Localization in Aluminum-Copper Single Crystals," *Acta Metall.*, Vol. 29, 1981, pp. 241-257.

2. Costin L. S., Chrisman, E. E., Hawley, R. H. and Duffy, J., "On the Localization of Plastic Flow in Mild Steel Tubes under Dynamic Torsional Loading," in: J. Harding (ed.), *Proc. 2nd Conference on Mechanical Properties at High Rates of Strain*, The Institute of Physics, Bristol and London, Conference Series No. 17, 1979, pp. 90-100.

3. Cox T. B. and Low, Jr., J. R., "An Investigation of the Plastic Fracture of AISI 4340 and 18 Nickel-200 Grade Maraging Steels," *Metall. Trans.*, Vol. 5, 1974, pp. 1457-1470.

4. Vardoulakis, I., "Bifurcation Analysis of the Triaxial Test on Sand Samples," *Acta Mechanica*, Vol. 32, 1979, pp. 35-54.

5. Vardoulakis, I., "Rigid Granular Plasticity Model and Bifurcation in the Triaxial Test," *Acta Mechanica*, Vol. 49, 1983, pp. 57-79.

6. Waversik, W. R. and Brace, W. F., "Post-Failure Behavior of a Granite and a Diabase," *Rock Mech.*, Vol. 3, 1971, p. 61.

7. Van Mier, J. G. M., "Strain-Softening of Concrete under Multiaxial Loading Conditions," Ph. D. Dissertation, De Technische Hogeschool Eindhoven, The Netherlands, 1984.

8. Hutchinson, J. W. and Tvergaard, V., "Surface Instabilities on Statically Strained Plastic Solids," *Int. J. Mech. Sci.*, Vol. 22, 1980, pp. 339-354.

9. Saje, M., Pan, J. and Needleman, A., "Void Nucleation Effects on Shear Localization in Porous Plastic Solids," *Int. J. Fract.*, Vol. 17, 1982, pp. 163-182.

10. Tvergaard, V., Needleman A. and Lo, K. K., "Flow Localization in the Plane Strain Tensile Test," *J. Mech. Phys. Solids*, Vol. 29, No. 2, 1981, pp. 115-142.

11. Tvergaard, V., "Ductile Fracture by Cavity Nucleation between Larger Voids," *J. Mech. Phys. Solids*, Vol. 30, 1982, pp. 265-286.

12. Needleman, A. and Tvergaard, V., "Finite Element Analysis of Localization in Plasticity," in: Oden, J. T. and Carey, G. F. (eds.), *Finite Elements - Special Problems in Solid Mechanics*, Vol. 5, 1982, pp. 95-267.

20

13. Hadamard, J., *Leçons sur la Propagation des Ondes et les Équations de L'Hydrodynamique*, Paris, Chp. 6, 1903.

14. Hill, R., "Acceleration Waves in Solids," *J. Mech. Phys. Solids*, Vol. 10, 1962, pp. 1-16.

15. Mandel, J., "Conditions de Stabilité et postulat de Drucker," in: Kravtchenko, J. and Sirieys, P. M. (eds.), *Rheology and Soil Mechanics*, Springer-Verlag, 1966, pp. 58-68.

16. Thomas, T. Y., *Plastic Flow and Fracture in Solids*, Academic Press, 1961.

17. Rice, J. R., "The Localization of Plastic Deformation," in: Koiter, W. T. (ed.), *Theoretical and Applied Mechanics*, North-Holland, 1976, pp. 207-220.

18. Prevost, J. H. and Hughes, T. J. R., "Finite-Element Solution of Elastic-Plastic Boundary Value Problems," *J. Appl. Mech., ASME*, Vol. 48, No. 1, 1981, pp. 69-74.

19. Prevost, J. H., "Localization of Deformations in Elastic-Plastic Solids," *Int. J. Num. Anal. Meth. Geomech.*, Vol. 8, 1984, pp. 187-196.

20. Willam, K. J., Bicanic, N. and Sture, S., "Constitutive and Computational Aspects of Strain-Softening and Localization in Solids," in: K. J. Willam (ed.), *Constitutive Equations: Macro and Computational Aspects*, ASME, New York, 1984, pp. 233-252.

21. Irons, B. M., "Numerical Integration Applied to Finite Element Methods," *Conf. on Use of Digital Computers in Structural Engineering*, Univ. of Newcastle, 1966.

22. Taylor, R. L., Beresford, P. J. and Wilson, E. L., "A Non-Conforming Element for Stress Analysis," *Int. J. Num. Meth. Engr.*, Vol. 10, 1976, pp. 1211-1219.

23. Pietruszcak, S. T. and Mroz, Z., "Finite Element Analysis of Deformation of Strain Softening Materials," *Int. J. Num. Meth. Engr.*, Vol. 17, 1981, pp. 327-334.

24. Nagtegaal, J. C., Parks, D. M. and Rice, J. R., "On Numerically Accurate Finite Element Solutions in the Fully Plastic Range," *Comp. Meth. Appl. Mech. Eng.*, Vol. 4, 1974, pp. 153-177.

25. Hughes, T. J. R., "Generalization of Selective Integration Procedures to Anisotropic and Nonlinear Media," *Int. J. Num. Meth. Eng.*, Vol. 15, 1980, pp. 1413-1418.

26. Rudnicki, J. W. and Rice, J. R., "Conditions for the Localization of Deformation in Pressure-Sensitive Dilatant Materials," *J. Mech. Phys. Solids*, Vol. 23, 1975, pp. 371-394.

27. Ortiz, M., "An Analytical Study of the Localized Failure Modes of Concrete," *J. Engr. Mech. Div., ASCE*, (to appear).

28. Belytschko, T. and Tsay, C. S., "A Stabilization Procedure for the Quadrilateral Plate Element with One-Point Quadrature," *Int. J. Num. Meth. Engr.*, Vol. 19, 1983, pp. 405-419.

29. Hughes, T. J. R., Liu, W. K. and Brooks, A., "Review of Finite Element Analysis of Incompressible Viscous Flows by the Penalty Function Formulation," *J. Comp. Phys.*, Vol. 30, 1979, pp. 1-60.

30. Strang, G. and Fix, G. J., *An Analysis of the Finite Element Method*, Prentice-Hall, 1973.

31. Simo, J. C. and Hughes, T. J. R., "On the Variational Foundations of Assumed Strain Methods," *J. Appl. Mech., ASME*, (to appear).

32. Drucker, D. C. and Prager, W., "Soil Mechanics and Plastic Analysis or Limit Design," *Q. J. Appl. Math.*, Vol. 10, 1972, pp. 157-165.

33. Hill, R., "A General Theory of Uniqueness and Stability in Elastic-Plastic Solids," *J. Mech. Phys. Solids*, Vol. 6, 1958, pp. 236-249.

34. Raniecki, B. and Bruhns, O. T., "Bounds to Bifurcation Stresses in Solids with Non-Associated Plastic Flow Laws at Finite Strain," *J. Mech. Phys. Solids*, Vol. 29, 1981, pp. 153-172.

35. O. C. Zienkiewicz, *The Finite Element Method*, Third Edition, McGraw-Hill, 1977, pp. 280-284.

Figure Captions

Figure 1 Close up view of the central portion of the shear band shown in Fig. 6.

Figure 2 Single element test problem.

Figure 3 Force-displacement curves computed from an isoparametric element, a $\bar{\bar{B}}$ method and the enhanced element.

Figure 4 Evolution of shear strains in test problem of Fig. 2. The results correspond to (a) $\bar{\bar{B}}$ method and (b) enhanced element.

Figure 5 Unit cell for a periodic distribution of voids subjected to an overall shear deformation.

Figure 6 Deformed mesh for the problem defined in Fig.5 at a prescribed shear strain $\bar{\gamma} = 0.0016$. Magnification factor for displacements $= 50$.

Figure 7 Distribution of bifurcated elements corresponding to the deformation shown in Fig. 6. The arrows represent the characteristic directions associated with the localized modes.

Figure 8 Distribution of effective plastic strain across the shear band at two stages of deformation. The values displayed are computed at the element centroids.

Figure 9 Plane strain punch problem on a tapered specimen. Deformed mesh for $\bar{u} = 0.4$.

Figure 10 Contours of maximum shear strain for punch problem shown in Fig. 9 at $\bar{u} = 0.4$. Results computed from (a) $\bar{\bar{B}}$ method and (b) enhanced element.

Figure 11 Plane strain soil specimen compressed between two rigid platens.

Figure 12 Load-displacement curve for problem shown in Fig. 11. Results computed from (a) isoparametric element and (b) enhanced element.

Figure 13 Deformed mesh computed from (a) isoparametric element and (b) enhanced element. The results correspond to points A and B on the load-displacement diagram, Fig. 12. Magnification factor for displacements $= 25$.

Figure 14 Contours of effective plastic strain computed from (a) isoparametric element and (b) enhanced element.

CLOSE UP OF SHEAR BAND

SHEAR BAND

STRAIN DISCONTINUITIES
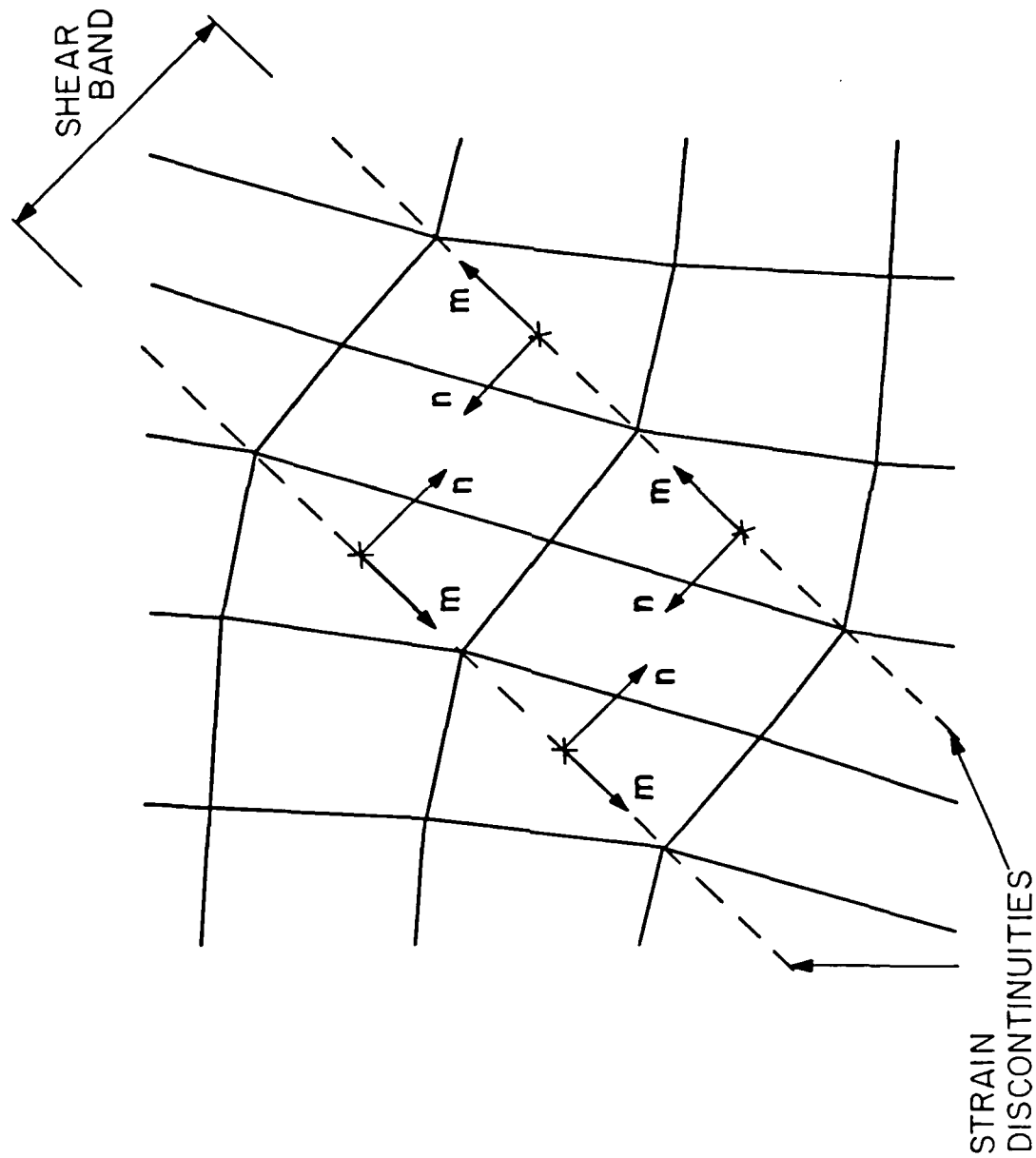
FIGURE 1

FIGURE 2

FIGURE 3

DISPLACEMENT u

SHEAR STRAIN
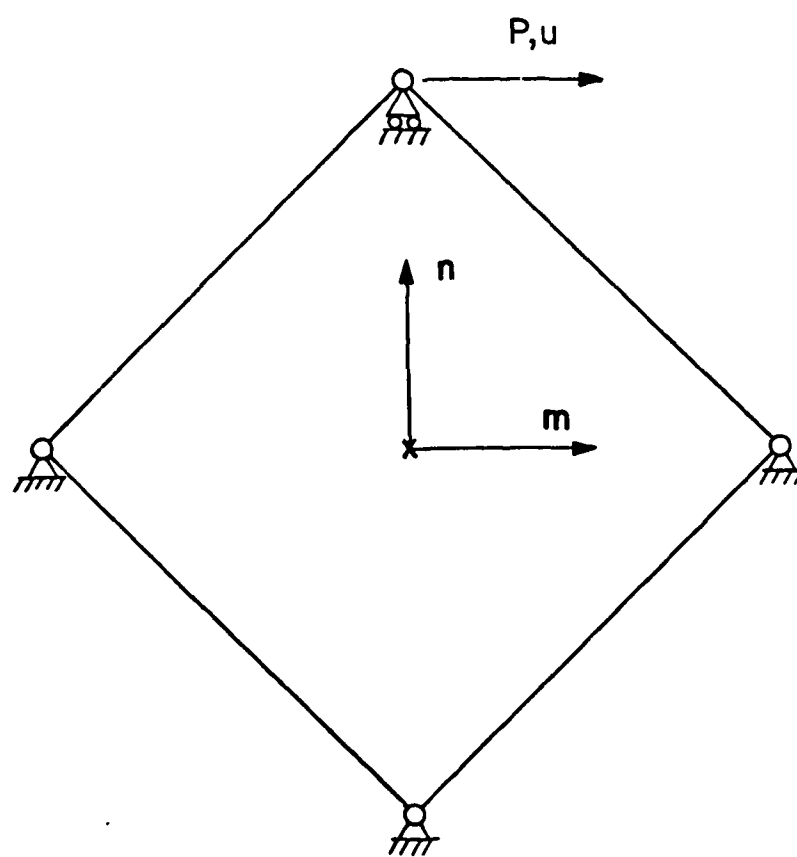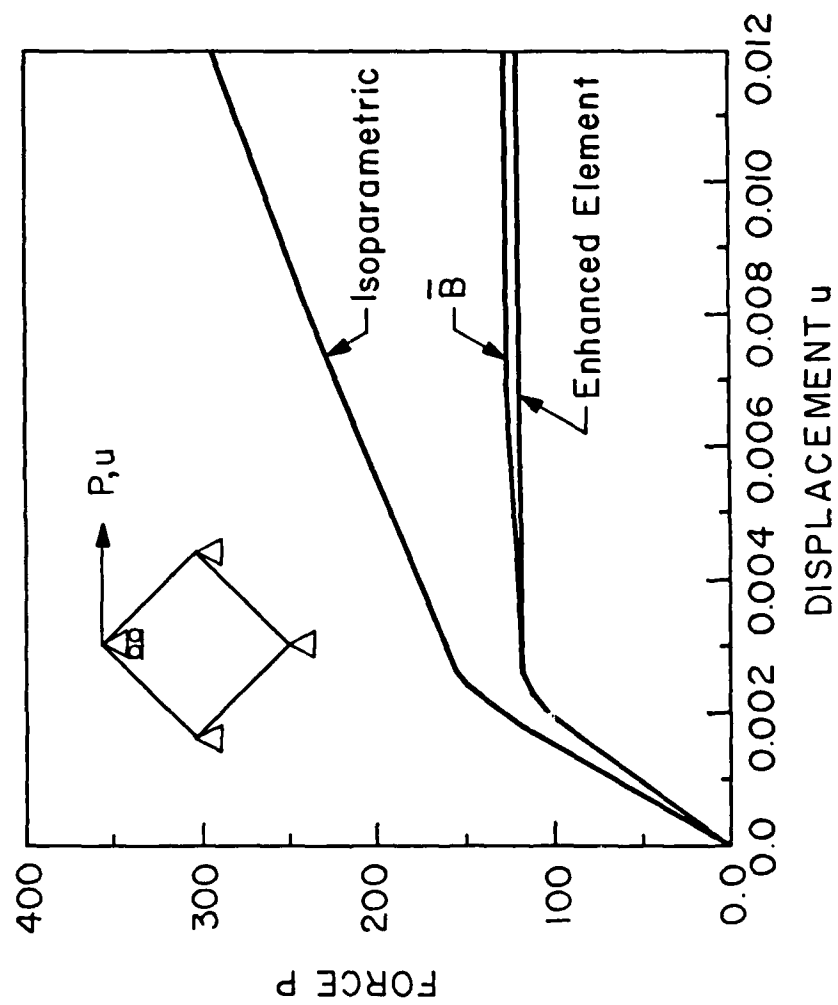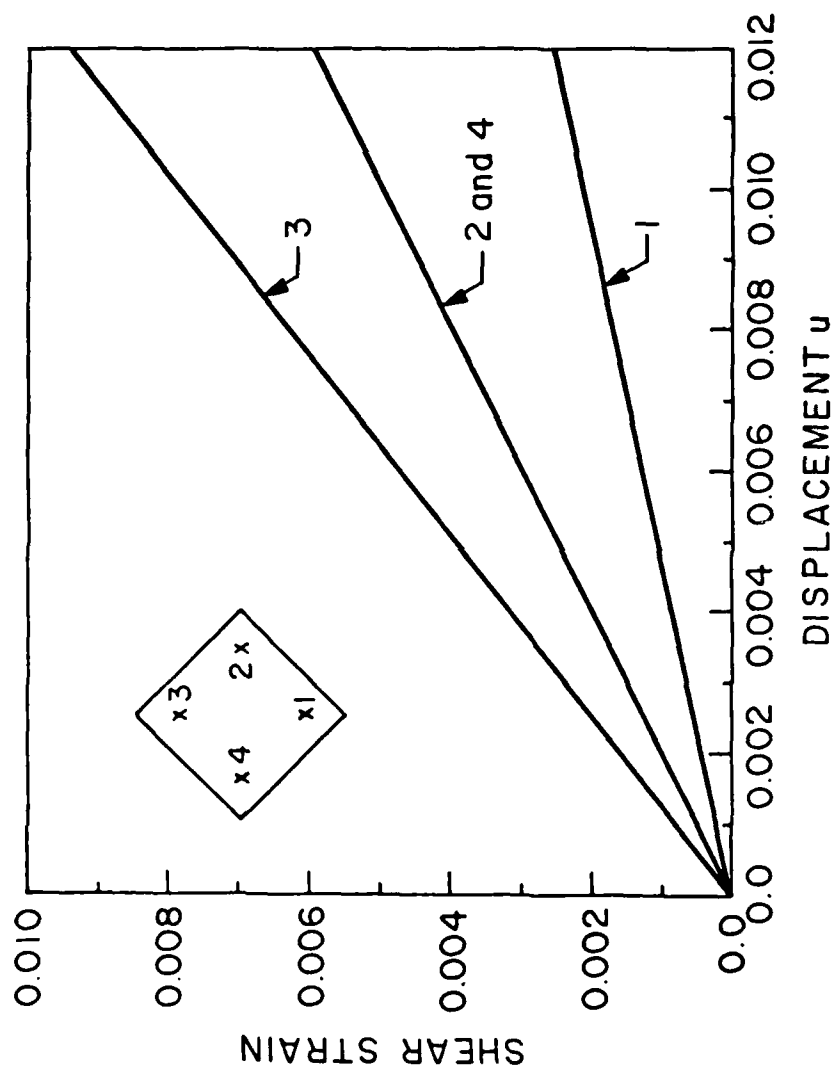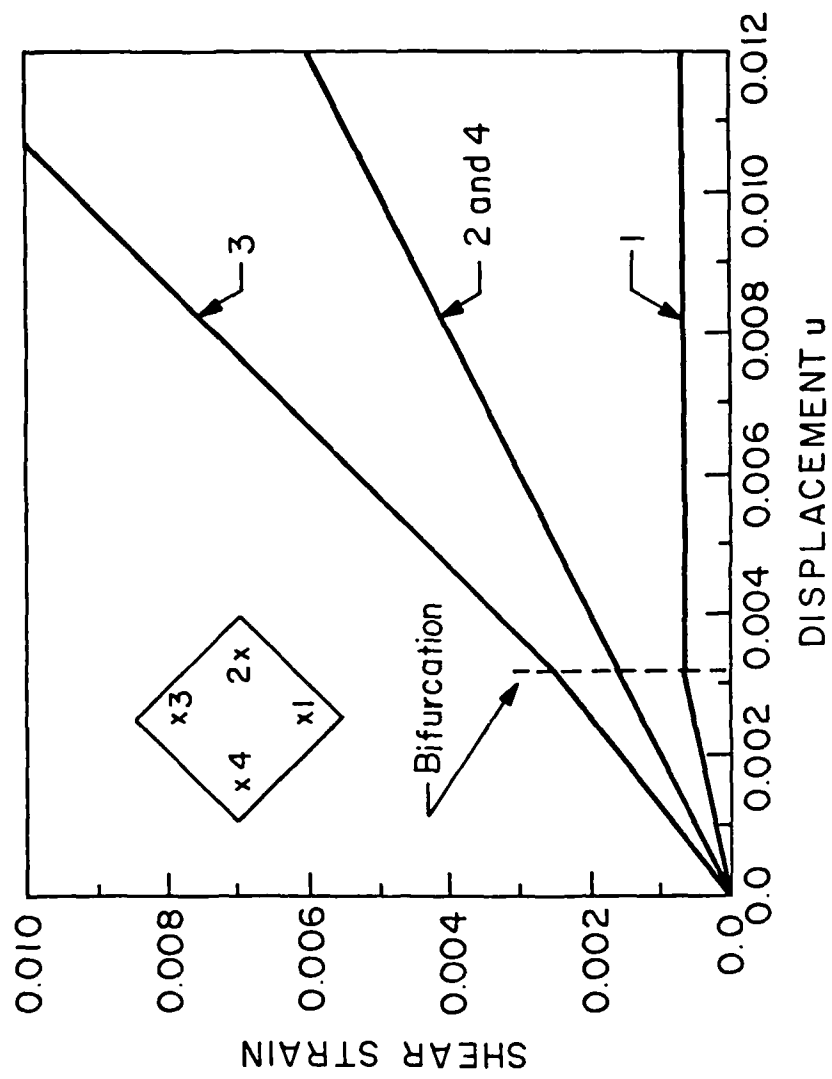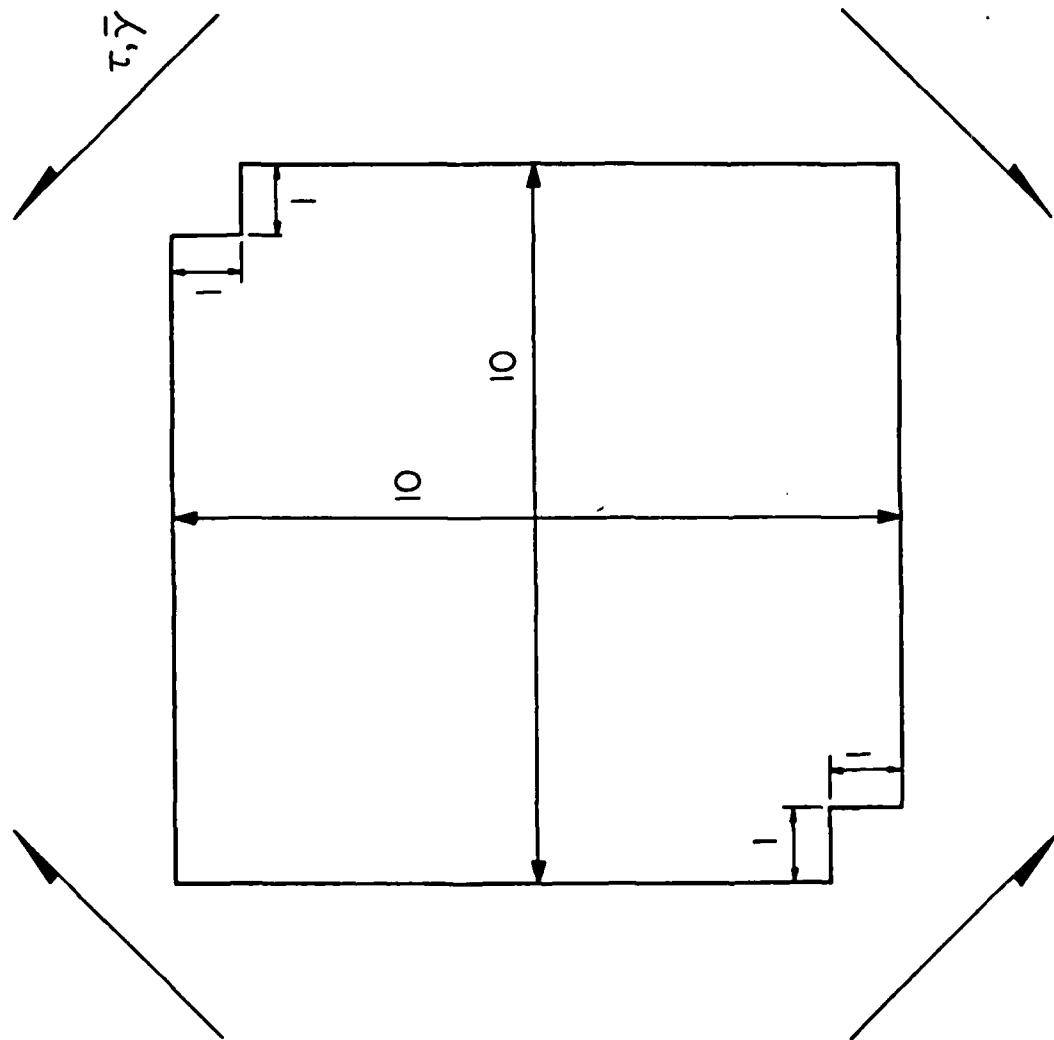
FIGURE 4a

FIGURE 4b

FIGURE 5
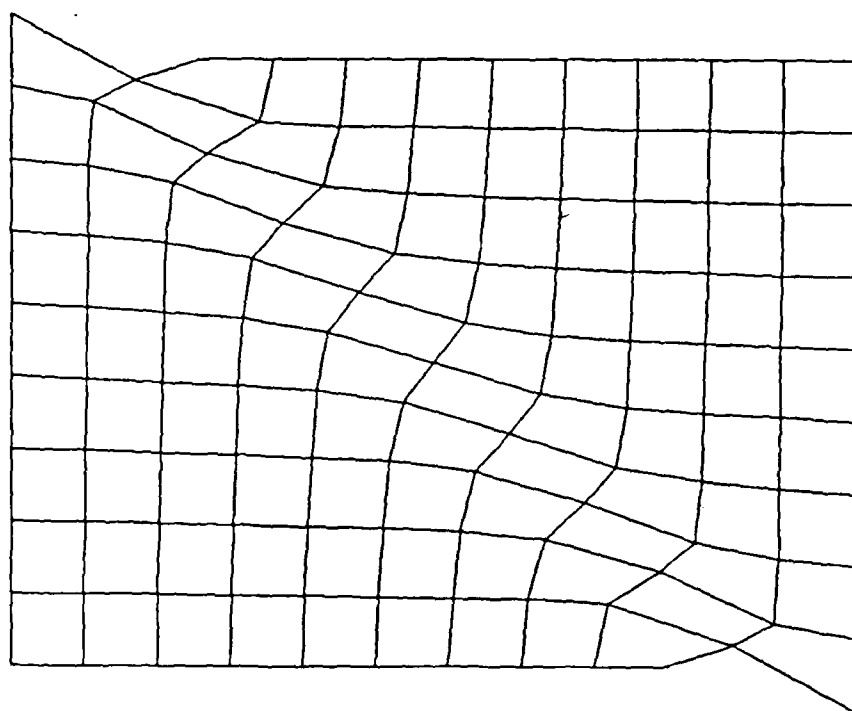
FIGURE 6
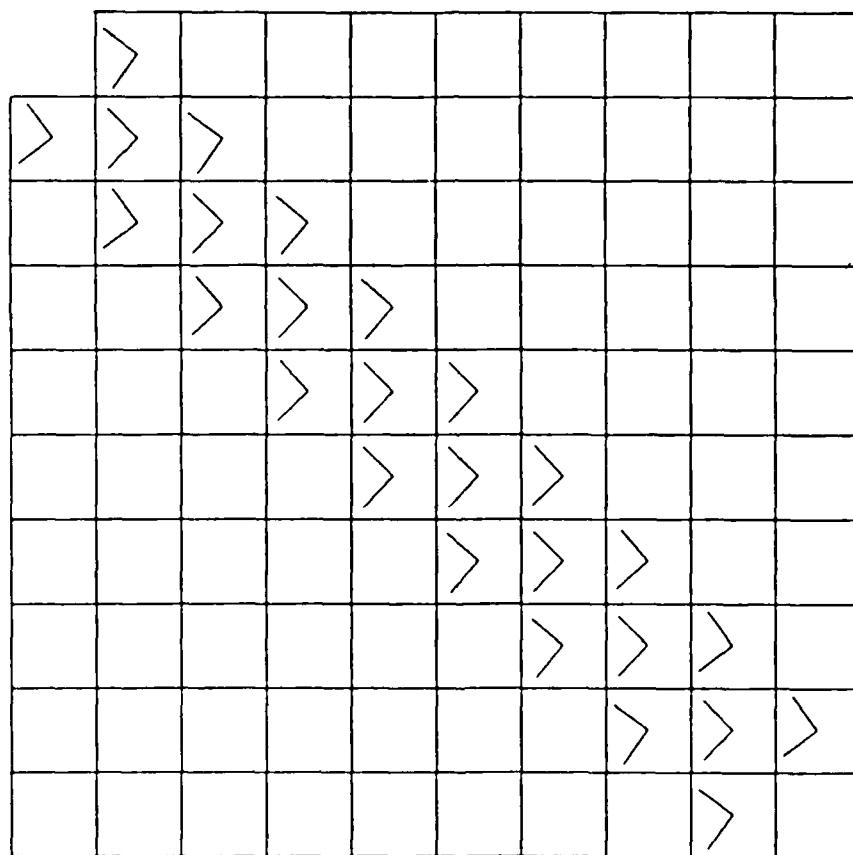
FIGURE 7
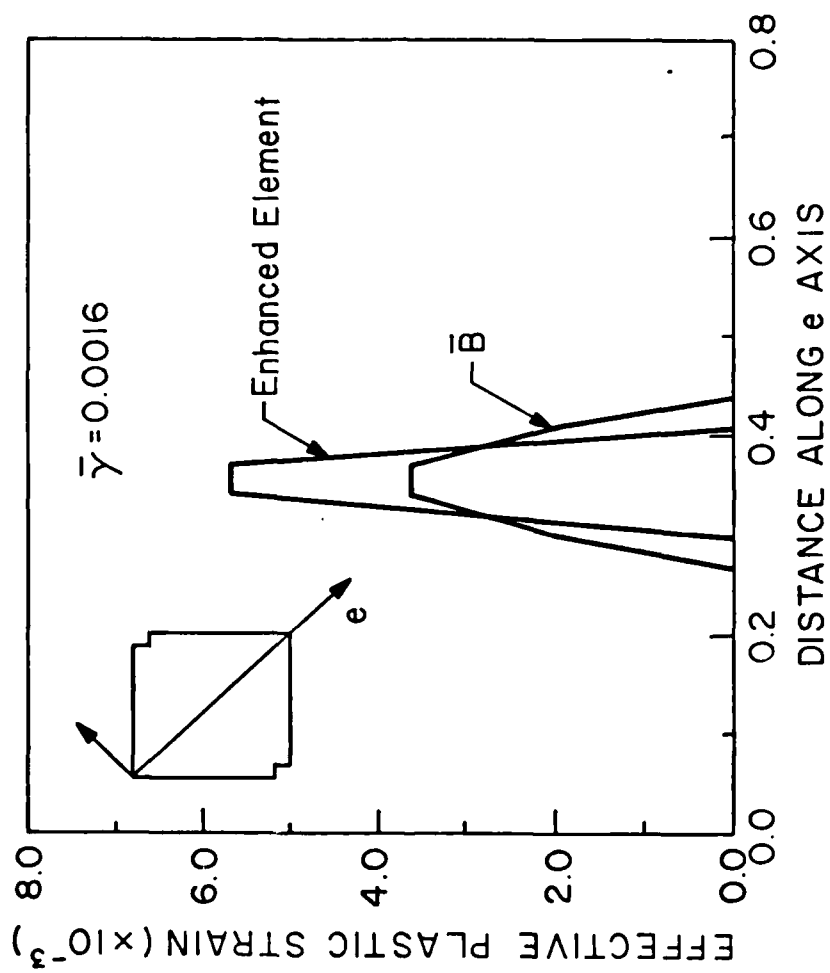
FIGURE 8a

FIGURE 8b

FIGURE 9

0.19

0.083
0.071
0.059
0.047
0.036
0.024
0.012

FIGURE 10a

0.33

0.14
0.12
0.10

0.086
0.069
0.051
0.034
0.017
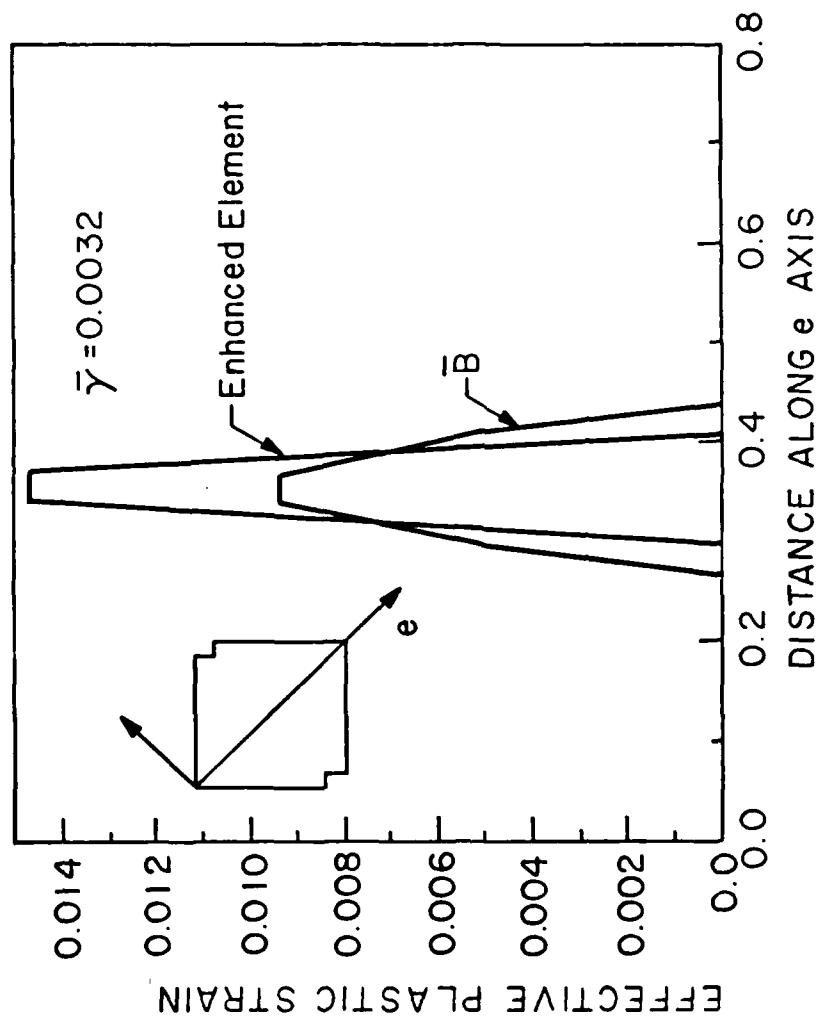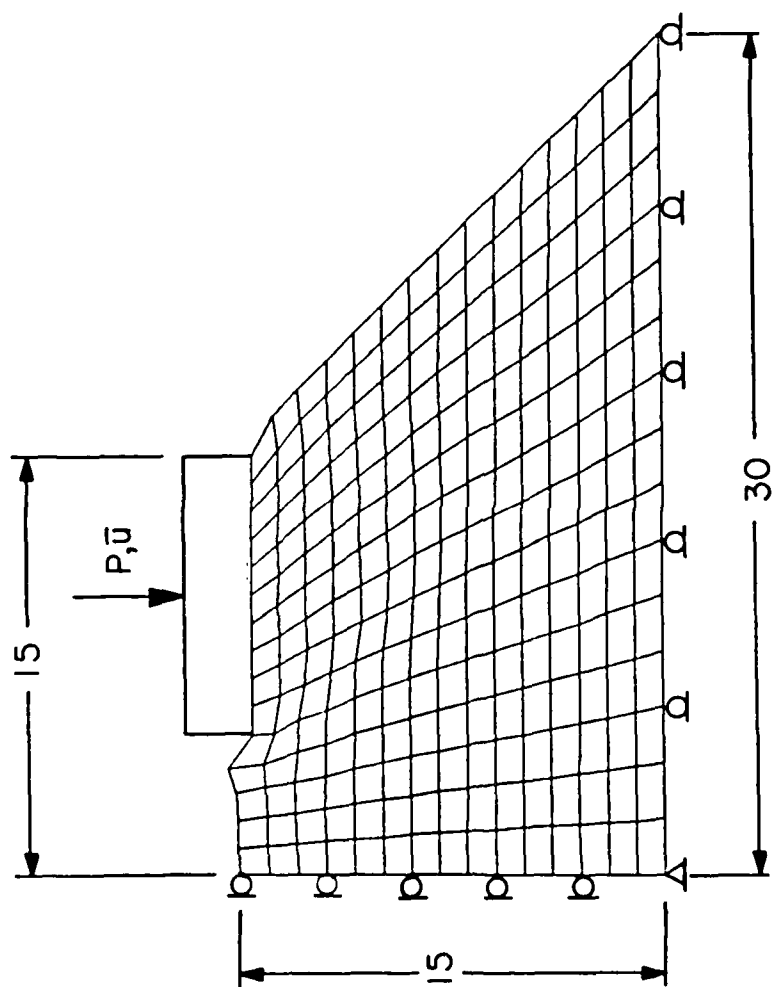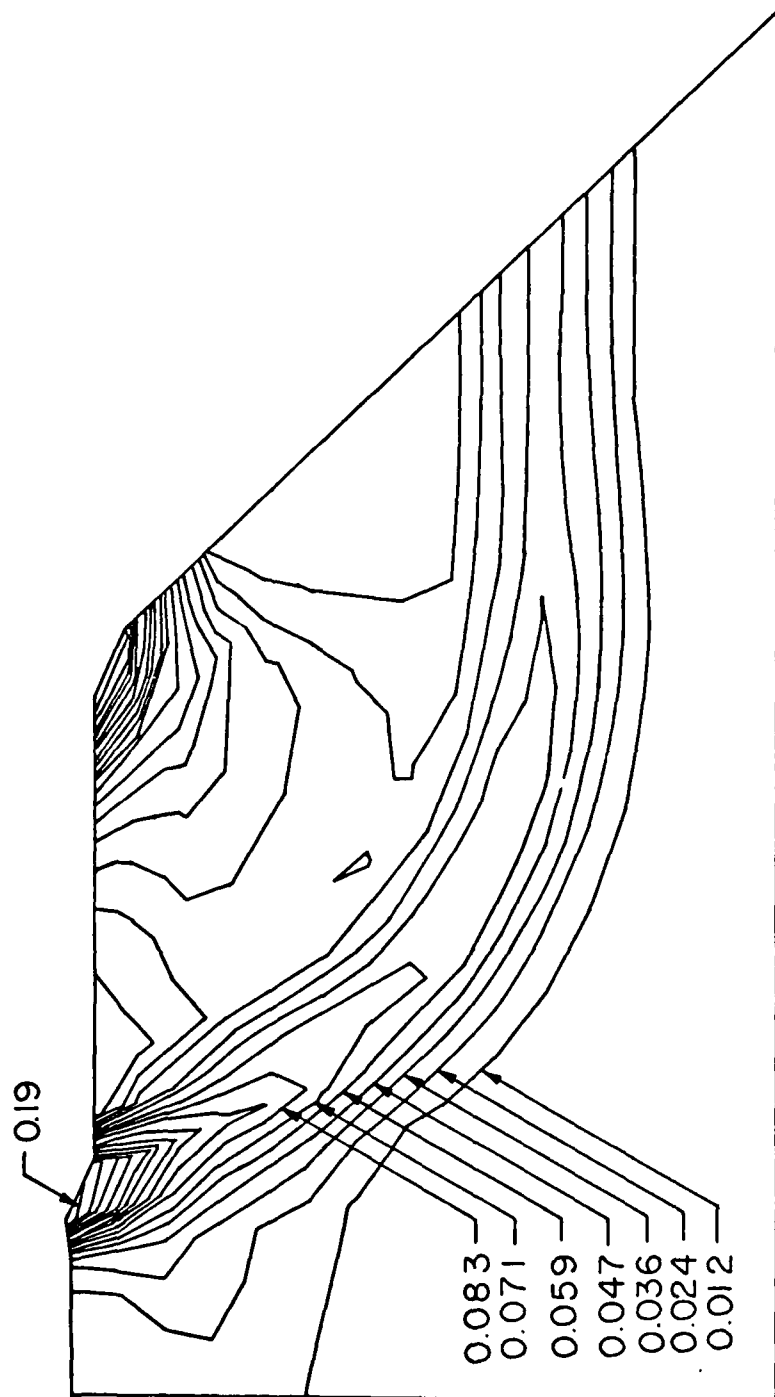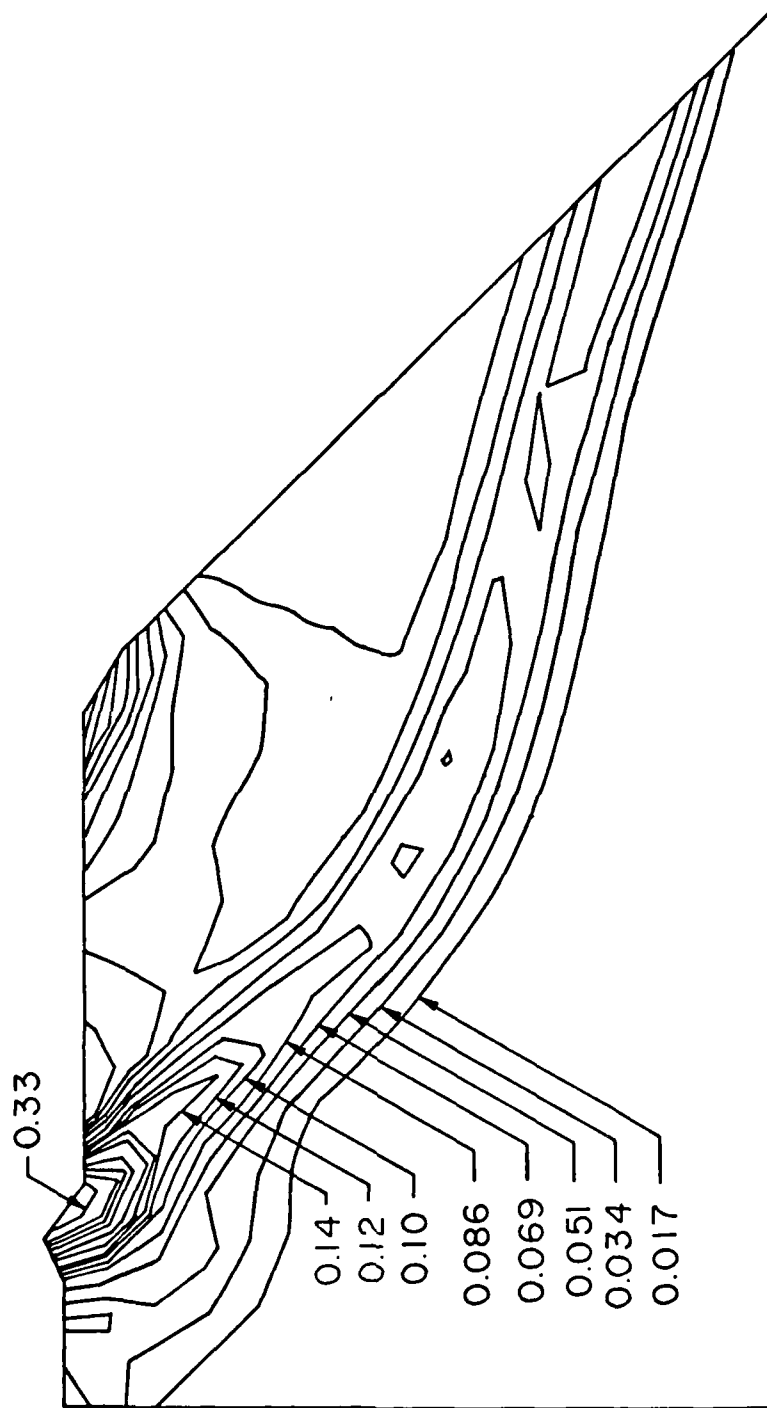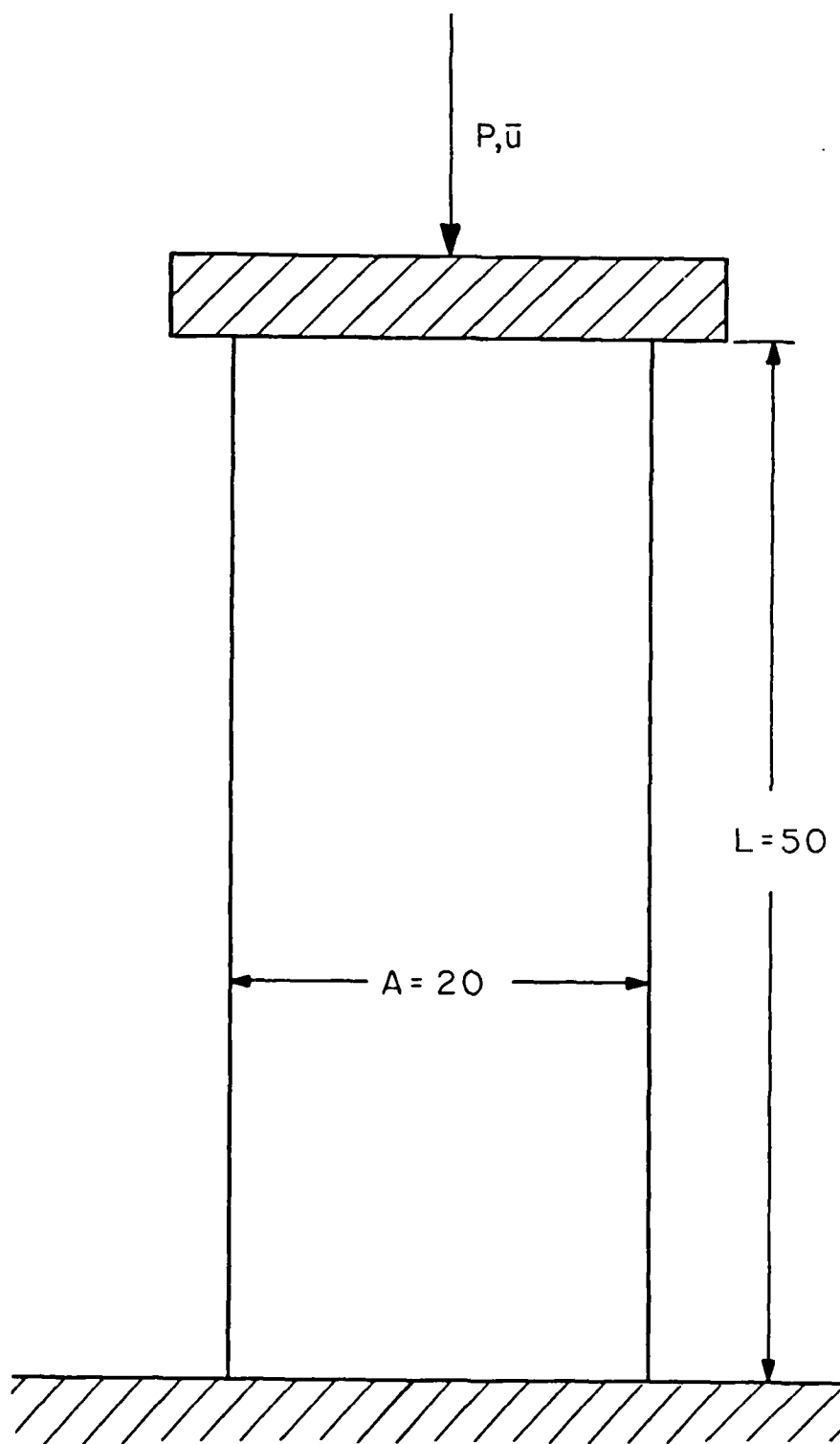
FIGURE 10b
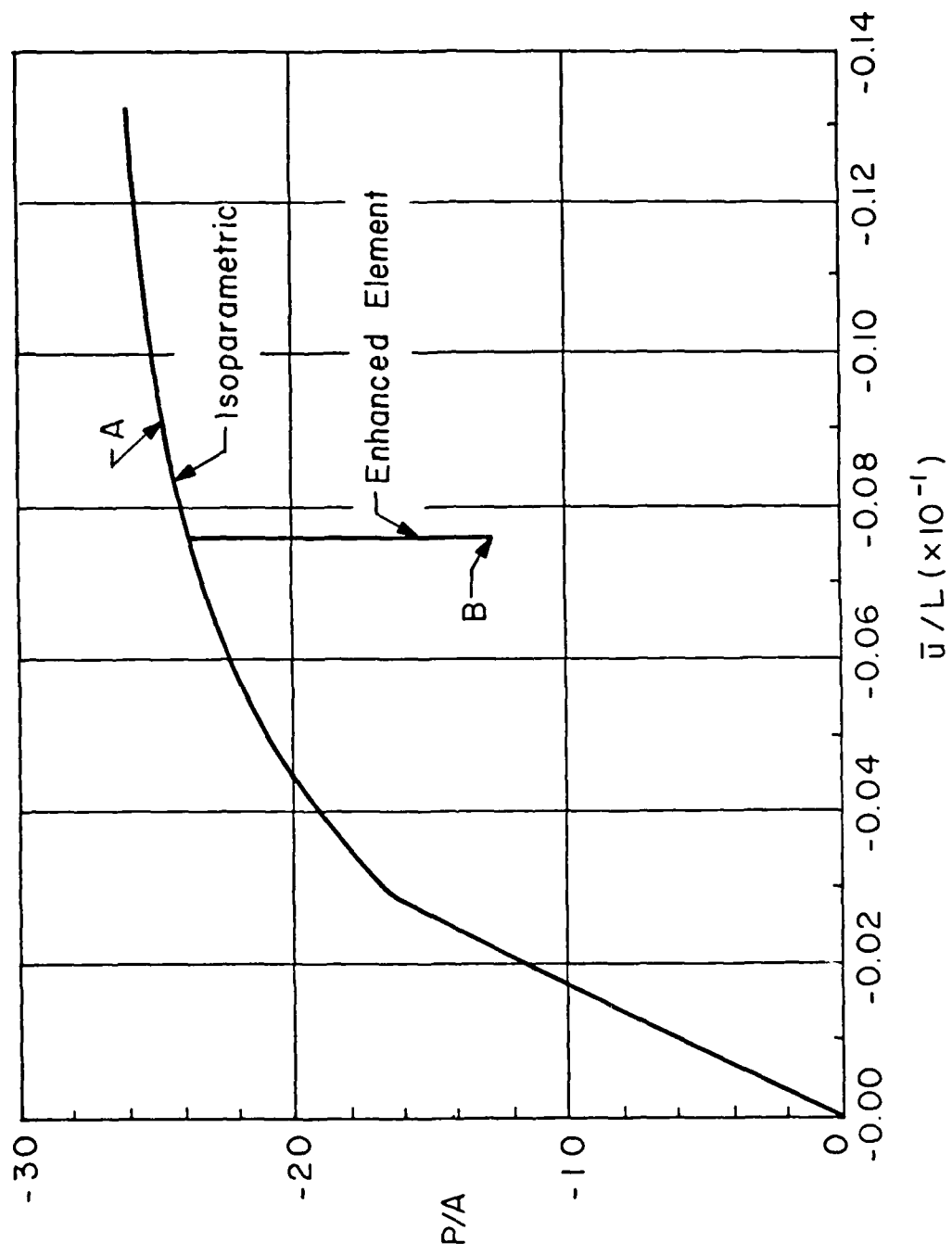
FIGURE 11

FIGURE 12
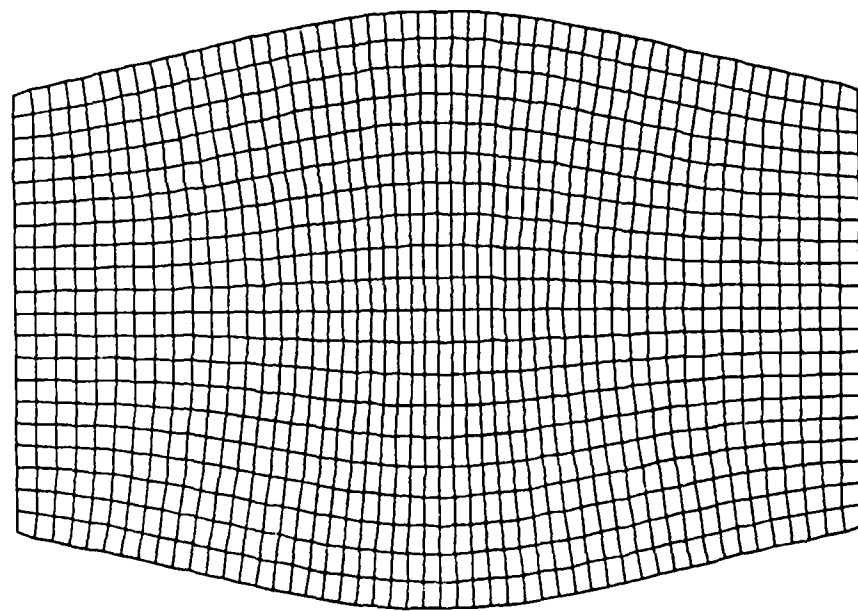
FIGURE 13a
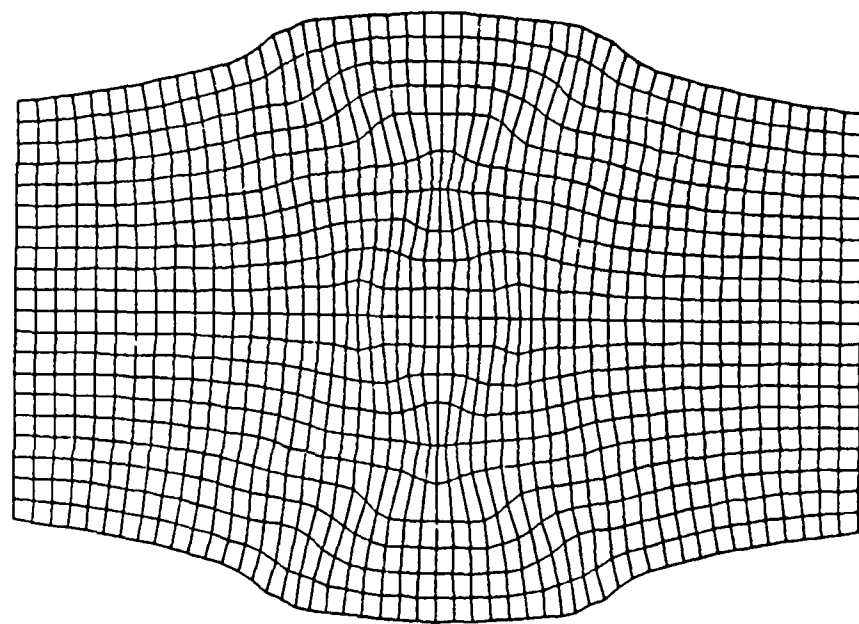
FIGURE 13b
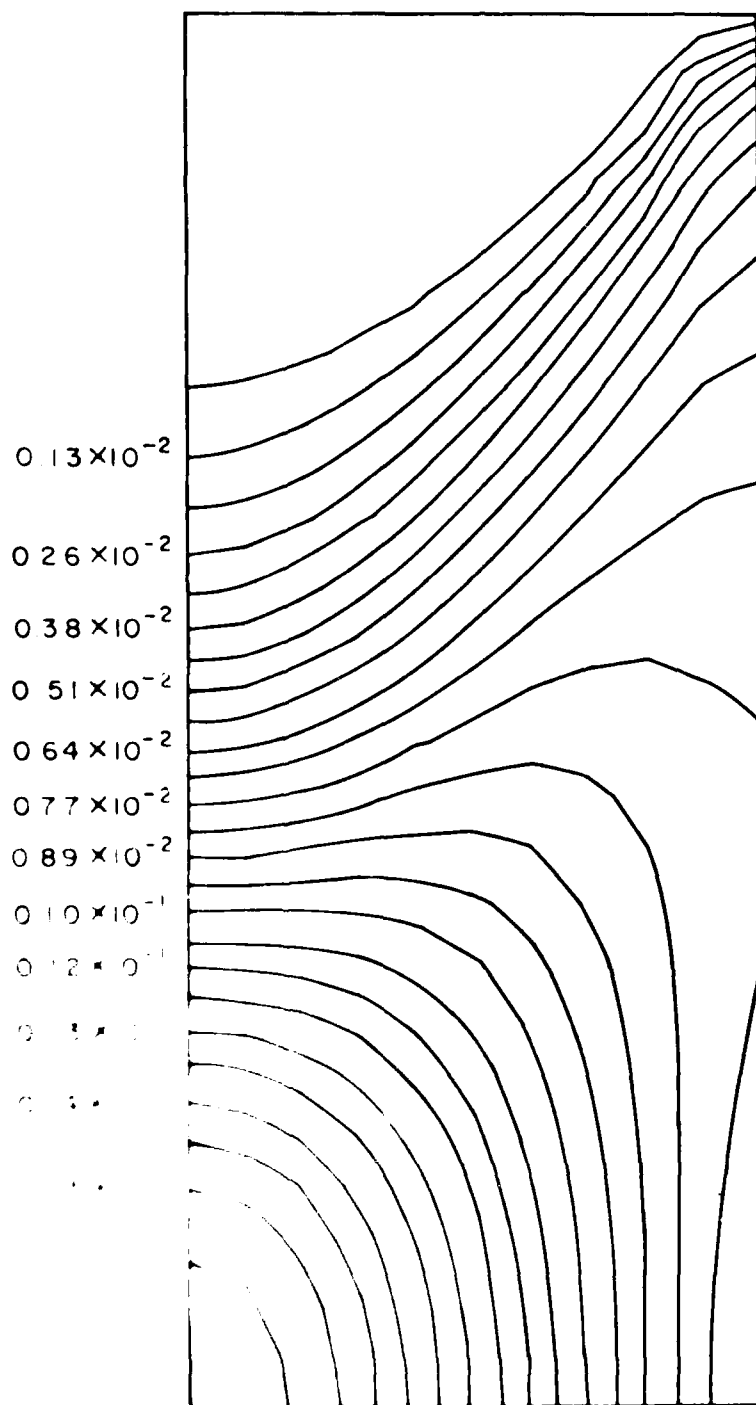
FIGURE 14a

FIGURE 14b

END

DTIC

7 — 86